

Catalysis Science & Technology

Accepted Manuscript



This is an *Accepted Manuscript*, which has been through the Royal Society of Chemistry peer review process and has been accepted for publication.

Accepted Manuscripts are published online shortly after acceptance, before technical editing, formatting and proof reading. Using this free service, authors can make their results available to the community, in citable form, before we publish the edited article. We will replace this *Accepted Manuscript* with the edited and formatted *Advance Article* as soon as it is available.

You can find more information about *Accepted Manuscripts* in the [Information for Authors](#).

Please note that technical editing may introduce minor changes to the text and/or graphics, which may alter content. The journal's standard [Terms & Conditions](#) and the [Ethical guidelines](#) still apply. In no event shall the Royal Society of Chemistry be held responsible for any errors or omissions in this *Accepted Manuscript* or any consequences arising from the use of any information it contains.

Cite this: DOI: 10.1039/c0xx00000x

www.rsc.org/xxxx

PAPER

Nitrogen-doped nanotubes-decorated activated carbon-based hybrid nanoarchitecture as superior catalyst for direct dehydrogenation†

Zhongkui Zhao,* Yitao Dai, and Guifang Ge

Received (in XXX, XXX) Xth XXXXXXXXXX 20XX, Accepted Xth XXXXXXXXXX 20XX

DOI: 10.1039/c0sc00000x

The novel N-doped activated carbon (AC) based nanostructure decorated with nanotubes (N-CNT-AC) has been successfully fabricated through a facile and scalable mechanical milling and subsequent solid pyrolysis approach of the low-cost and commercially available AC and melamine. Various characterization techniques including high resolution transmission electron microscopy, X-ray diffraction, Nitrogen adsorption, X-ray photoelectron spectroscopy, Raman spectroscopy and Fourier Transform infrared spectroscopy were employed to reveal the relationship between catalyst feature and catalytic performance in the oxidant- and steam-free direct dehydrogenation (DDH) of ethylbenzene to styrene. Although the as-synthesized AC-based hybrid nanostructure has a much lower surface area ($397.0 \text{ cm}^2 \text{ g}^{-1}$) and pore volume ($0.17 \text{ cm}^3 \text{ g}^{-1}$) than those of parent AC ($777.1 \text{ cm}^2 \text{ g}^{-1}$ surface area and $0.4 \text{ cm}^3 \text{ g}^{-1}$ pore volume), it demonstrates 1.74 and 3.67 times the steady-state styrene rate of the per gram parent AC and the industrially used K-Fe catalyst, respectively, for the DDH reaction, ascribed to the promoting effect of the unique hybrid microstructure, surface rich C=O group and defect/edge feature, the increased basic properties through N-introducing into the hybrid nanostructure, small size of graphitic crystallite, as well as the inherent high surface and large porosity of AC-based materials. The in situ Fourier Transform infrared spectroscopy measurement suggests the lower activation energy over the developed novel N-doped AC-based hybrid nanostructure for DDH reaction than that over the parent AC. Interestingly, the developed hybrid nanocomposite exhibits much superior selectivity for styrene production to the parent AC, ascribed to the N-doping into the AC-based matrix. The developed N-doped AC-based hybrid nanostructure catalyst could be a potential candidate for catalytic styrene production via steam- and oxidant-free direct dehydrogenation of ethylbenzene.

Introduction

The development of low-cost sustainable catalysts with high catalytic activity, selectivity, and stability under mild conditions remains at the heart of modern material chemistry, green chemistry, and catalysis fields for academic and practical aspects.¹⁻³ Although the metal catalysts have currently been playing major roles in various industrial transformation processes, they still suffer from many inherent disadvantages such as low-availability, high cost, susceptibility to gas poisoning, detrimental effects on our environment, besides the residual metal in products.⁴⁻⁷ Owing to the broad availability, environmental acceptability, corrosion resistance, and unique surface properties, nanocarbon materials have been demonstrated to be promising and sustainable low-cost metal-free alternative to metal-based catalysts for organic synthesis,⁸⁻¹⁴ hydrogen production,^{15,16} photodegradation of organic pollutants,^{17,18} the crucial oxygen reduction reaction in fuel cells,¹⁹⁻²¹ and as counter electrode catalyst for solar cells.^{22,23} Nowadays, the carbocatalysis has already attracted great attention throughout the world, and

become the foreland and hot topic in the heterogeneous catalysis and sustainable chemistry. However, the low-cost and facile large-scale production of the nanostructured carbon materials for industrial application is highly desirable but remains a challenge. AC is a common carbon material that can be facilely and economically produced from various carbonaceous sources such as wood, nutshells, coconut husk, peat, lignite, coal, and petroleum pitch.²⁴ The high surface area ($>1000 \text{ m}^2 \text{ g}^{-1}$), large porosity ($>0.5 \text{ cm}^3 \text{ g}^{-1}$), as well as abundance, low cost, renewability, environmental compatibility, corrosion resistance endows it to be a potential candidate for industrially-used catalyst, besides the other applications such as energy conversion and storage, CO₂ capture, environmental protection and water purification.²⁵⁻²⁹ Generally, AC is employed as an efficient support for many catalysts including industrially used ones, i.e. supported silicotungstic acid catalyst on AC, Pd/C, etc.³⁰⁻³⁵ AC have been employed as metal-free catalysts for various reactions including oxidative dehydrogenation of hydrocarbon.³⁶⁻³⁹ However, the depressed selectivity, low catalytic activity and poor stability limit it to be lonely performed as a practical catalyst.⁴⁰ Therefore, a powerful strategy for improving the

catalytic activity, selectivity and stability of AC-based metal-free catalysts is highly desirable but still remains a huge challenge. The catalytic performance of carbon materials strongly depends on their microstructure. The nanostructured carbon materials exhibit high catalytic performance including activity, selectivity, and stability, and have been considered to be an alternative to metal-based catalysts.^{5-7,40,41} However, the high cost and complex preparation process for the production of the established nanostructured carbon materials such as graphene, carbon nanotube, fullerene and their composites inhibit it from using as practical industrially-used catalysts. Therefore, the fabrication of AC-based nanostructured carbon materials from a low-cost and extensively available AC parent by a facile and economic preparation method may be a sapiential strategy for developing practical and highly-efficient metal-free catalysts in diverse transformations.

Dehydrogenation of ethylbenzene to styrene is one of the commercially important reactions in chemical industry. Styrene is mainly used as monomer in the production of polystyrene and several copolymers. At present, the process of ethylbenzene dehydrogenation is industrially carried out over Fe-K-Cr oxide-based catalysts.⁴² The commercial catalyst shows several advantages such as low cost and high resistance against impurities, but it has some disadvantages like quick deactivation due mainly to potassium loss, unstable Fe³⁺ state, coke-deposition, as well as the caused health injuries to human beings due to the existing chromium in this system. Moreover, the introduction of superheated steam into the feed is indispensable, which can efficiently inhibits the quick deactivation due to coke-deposition, but much energy is wasted.^{43,44} The search for new catalyst systems with high stability of Fe³⁺ species and coke-resistance in the absence of potassium or steam is highly required, but a large breakthrough on these issues is in an extremity although many efforts have been made.⁴⁵⁻⁴⁷ Therefore, some alternative routes such as side-chain alkylation of toluene with methanol and molecular oxygen-assisted oxidative dehydrogenation of ethylbenzene have been proposed, but they demonstrate either insufficient selectivity or risks in handling flammable mixtures.^{8,40,48-50} The oxidant- and steam-free DDH reaction is a fascinating approach with energy-saving, clean and safe features for styrene production. The DDH reaction of ethylbenzene to styrene under oxygen- and steam-free conditions was reported by using nanodiamond as an efficient metal-free catalyst,⁵¹ which makes sail the studies on developing carbon-based catalyst for this reaction. Recently, the core-shell sp²/sp³ composite structured hybrid nanocarbon was demonstrated as an active and selective catalyst for DDH of propane to propene. It was found that the optimum catalytic activity depends on the maximum structural defectiveness and high chemical reactivity of the ketone groups. In our previously reported papers,⁵² we have demonstrated that the introduction of nitrogen into carbon structure can efficiently enhance the catalytic properties including activity and selectivity for DDH of ethylbenzene to styrene under oxidant- and steam-free conditions. The lone electron pairs of nitrogen atoms can form a delocalized conjugated system with the sp²-hybridized carbon frameworks to change electronic behaviour and also can produce defect sites on carbon surface resulting in great improvement of the reactivity,^{19,20} as well as the

introduction of N can improve the basic properties of carbon materials resulting in promotion in dehydrogenation activity but inhibition in cracking side reaction of ethylbenzene by decreasing the amount of phenolic hydroxyl group.^{12,39,51,53-55} The carbon material catalyzed direct dehydrogenation under oxygen- and steam-free conditions have been demonstrated to be a fascinating alternative for styrene production from the viewpoint of energy-saving, environmental protection and economic issues.^{41,51,52} We also found that the CN_x layer coated on nanodiamond exhibits much superior catalytic performance to the parent nanodiamond. Therefore, we envision that the catalytic properties of AC can be hopefully improved by fabricating N-doped AC-based hybrid nanostructures decorated nanotubes, resulting in an efficient and practical catalyst for DDH reaction. However, there are no report on the fabrication of N-doped AC-based hybrid can be found.

In this work, the novel N-doped AC-based hybrid nanostructure decorated with nanotubes has been successfully fabricated through a facile mechanical milling and subsequent solid pyrolysis approach of the low-cost commercially available AC and melamine (Fig. 1). To the best of our knowledge, this is the first report on the successful fabrication of the N-doped nanotubes decorated AC-based hybrid nanostructure. The catalytic performance of N-doped AC-based hybrid prepared with 1:10 of AC/melamine at 850 °C demonstrates 1.74 and 3.67 times the steady-state styrene rate of the parent AC and the industrially used K-Fe catalyst, respectively, for the DDH of ethylbenzene to styrene under oxidant- and steam-free conditions. The obtained N-doped AC-based hybrid nanostructure and the parent AC have been characterized by employing sophisticated techniques such as X-ray diffraction (XRD), high-resolution transmission electron microscopy (HRTEM), X-ray photoelectron spectroscopy (XPS), Fourier transform infrared spectroscopy (FT-IR), Raman spectroscopy, and in situ FT-IR experiments. Incorporating the reaction results with the characterization results, we found that the much superior catalytic performance of the N-doped AC-based hybrid nanostructure to the parent AC for DDH reaction can be ascribed to the promotion effect of the unique hybrid nanostructures named as microstructure effect, surface rich C=O group and defect/edge feature, increased basic properties through N-introducing into the hybrid nanostructure, small size of graphitic crystallite, as well as the inherent high surface and large porosity of AC-based materials. Interestingly, the developed

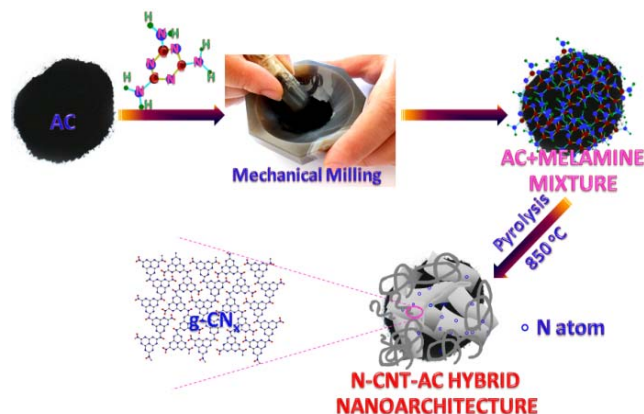


Fig. 1 Schematic illustration for the fabrication of N-doped AC-based hybrid nanostructure fabricated through a facile pyrolysis approach.

hybrid composite exhibits much superior selectivity for styrene production to the parent AC, ascribed to the N-doping into the AC-based matrix. The developed AC-based hierarchical hybrid nanostructure can be hopefully used as efficient catalysts in diverse reactions as well as employed to be a practical candidate for many other applications such as solar cell, CO₂ capture, hydrogenation storage, supercapacitor, oxygen reduction, etc. owing to its N-doping, unique structure, and the inherent high surface area and large porosity of AC-based materials, now that AC and N-doping AC have demonstrated excellent application properties in above fields.²⁵⁻²⁹

Experimental section

Preparation of N-doped AC-based hybrid nanostructure

The commercially supplied AC derived from coconut shells (Aladdin Chemical Co., for catalyst support, China) was finely ground with melamine in an agate mortar (1:10), and then heated up to the 850 °C in N₂ atmosphere at the certain ramp rate to obtain the final nanotube decorated N-doped hybrid nanostructured carbon (Fig. 1). For comparison, the AC was calcined under the same conditions as above except for the absence of melamine.

Characterization of the catalyst

X-ray diffraction (XRD) profiles were collected from 10 to 80° at a step width of 0.02° using Rigaku Automatic X-ray Diffractometer (D/Max 2400) equipped with a CuKα source ($\lambda = 1.5406 \text{ \AA}$). TEM images were obtained by using Tecnai F30 HRTEM instrument (FEI Corp.) at an acceleration voltage of 300 kV. SEM experiments were performed on JEOL JSM-5600LV SEM/EDX instrument. The XPS spectra were carried out on an ESCALAB 250 XPS system with a monochromatized Al Kα X-ray source (15 kV, 150 W, 500 μm , pass energy = 50 eV). FT-IR spectroscopy characterization of catalysts was performed at 150 °C under ultrahigh vacuum using a Bruker EQUINOX55 infrared spectrometer. The Raman spectra were measured using a laser with an excitation wavelength of 532 nm at room temperature on a Thermo Scientific DXR Raman microscope. FT-IR spectroscopy characterization of catalysts was performed at 150 °C under ultrahigh vacuum using a Bruker EQUINOX55 infrared spectrometer. Nitrogen adsorption and desorption isotherms were determined on a Micromeritics apparatus of model ASAP-2020 system at -196 °C. The specific surface areas were calculated by the BET method. In situ FT-IR experiments were conducted on the same IR instrument, the sample was degassed at 150 °C under ultrahigh vacuum for 30 min, and then ethylbenzene was injected into the environmental chamber with the temperature of chamber increased from 150 to 400 °C at a heating rate of 5 °C min⁻¹, and the infrared spectrums were recorded per 5 minutes.

Measurement of catalytic performance

Direct dehydrogenation of ethylbenzene was performed at 550 °C for 20 hours in a stainless steel, fixed bed flow reactor (6 mm O.D.) at atmospheric pressure. 25 mg catalyst was loaded at the centre of the reactor with two quartz wool plugs at its two sides. The system was heated to 600 °C and kept for 30 min in Ar for pretreating catalyst. After the system was cooled down to 550 °C and kept for 10 min, the feed containing 2.8% ethylbenzene with

a flow rate 10 ml min⁻¹ and Ar as balance was then fed into the reactor from a saturator kept at 40 °C. The effluent from the reactor was condensed in two traps containing certain amount of ethanol connected in a series. The condensed material was cooled externally in an ice water bath. Quantitative analysis of the collected reaction products (ethylbenzene, styrene, toluene, and benzene) was performed on a FULI 9790 II GC equipped with HP-5 column, 30 m×0.32 mm×0.25 μm , and FID detector. The resulting carbon balance was above 100±4% in all reactions. The styrene rate and selectivity of styrene are employed as the evaluation standard for the catalytic performance of the fabricated N-doped AC-based hybrid composites. The styrene rate is calculated as the formed styrene molar amount per g catalyst per hour, and the selectivity of styrene is denoted as the percentage of the desired styrene to the total products including the desired styrene and the by-products that containing benzene and toluene. For comparison, the catalytic properties of the calcined AC (suffering from the same calcination procedure as that for preparing N-doped AC-based hybrid nanostructure), mesoporous CN_x, and the industrially-used K-Fe catalysts (commercially provided by Haitai Tech. Ltd. China) were also measured. In all cases, the used AC for characterization and catalytic performance test is the calcined activated carbon at 850 °C in N₂.

Results and discussion

Morphology and structure feature of N-doped AC-based hybrid nanostructure

Activated carbon is a commercially available common carbon material in large scale, and therefore the development of AC-based nanostructured materials using the abundant, low-cost and renewable AC as starting material is highly essential for diverse practical applications. In this work, we expected to fabricate AC-based nanostructured hybrid composite through a facile and economic mechanical milling and subsequent controllable

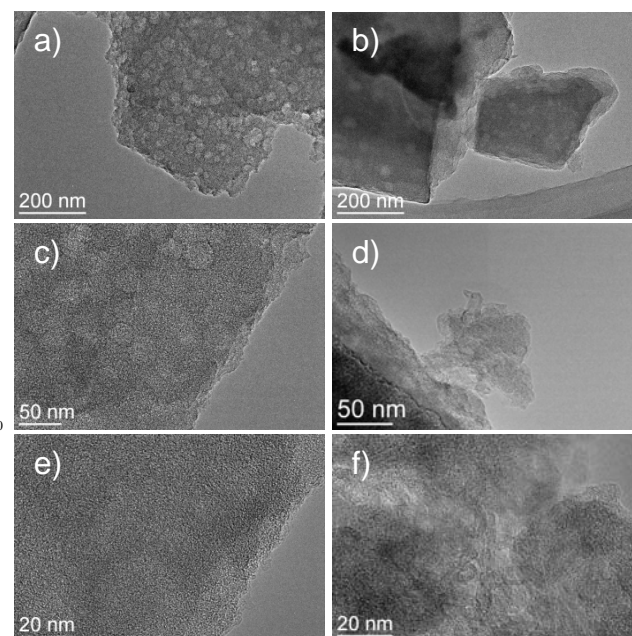


Fig. 2 TEM images of the parent AC (a,c,e) and the as-prepared N-doped AC-based hybrid nanostructure (b,d,f).

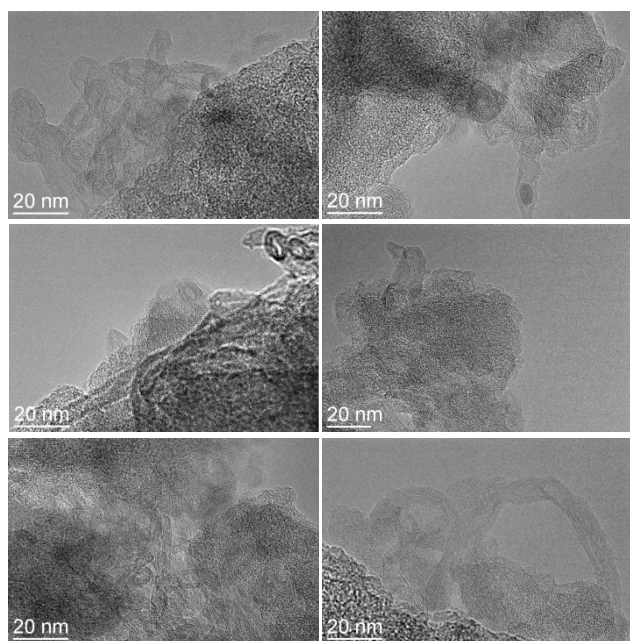


Fig. 3 HRTEM images at different regions of the as-prepared N-doped AC-based hybrid nanostructure.

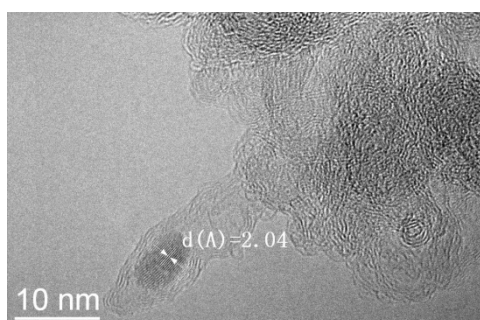


Fig. 4 HRTEM images of the as-prepared N-doped AC-based hybrid nanostructure.

pyrolysis approach. The typical TEM images (Fig. 2) of the synthesized N-doped AC-based hybrid nanostructure and the parent AC reveal the formation of the AC-based hybrid nanoarchitecture. In comparison with the parent AC (Fig. 2a), the number of nanopores on the formed carbon materials becomes fewer (Fig. 2b), suggesting the partial pores being filled by the possible CNx.⁴¹ TEM image for the pores becomes faintness (Fig. 2c), further indicating the possible existence of surface CNx nanosheet. In order to confirm that the porous structure disappeared after the CNx was formed on AC surface, nitrogen adsorption experiments were done. The decreasing surface area (397.0 m² g⁻¹) and pore volume (0.17 cm³ g⁻¹) of N-CNT-AC in comparison to AC (777.1 m² g⁻¹ and 0.40 cm³ g⁻¹ for surface area and pore volume, respectively) further unambiguously confirms the above conclusion drawn from TEM that the formed CNx layer covering on AC surface. More interestingly, from Fig. 2d, we can clearly see a bird-like nanostructure fabricated from some nanotubes growing on the AC, and furthermore we observe many nanotubes with diverse tube diameters growing on the different regions of the as-prepared materials by changing the TEM focusing position (Fig. 2f, Fig. 3). The nanotubes have randomly twisted into different shapes like bird and others (Fig. 3). Then in

order to explore why the CNx can be formed, we observed the sample by HRTEM (Fig. 4), and the Ni (PDF#: 45-1027, d(011)=2.04 Å) or Fe (PDF#: 85-1410, d(110)=2.04 Å) or Co (PDF#: 15-0806, d(111)=2.04 Å) nanocrystallite on the top of multiwall nanotube can be observed, which may catalyze the growth of nanotube on AC surface. We can suppose that the contained metal in AC may improve its catalytic performance. Therefore, we performed the control experiment on the diluted acid treated AC, but we cannot find any difference in catalytic performance between the acid washed and unwashed AC. We can conclude that the too low content of metal doesn't change the catalytic performance of AC. Moreover, neither AC nor the developed hybrid material from AC in Fig. 10 suffered acid washing treatment. Therefore, we can safely say that the N-doped AC-based hybrid nanostructure demonstrates superior catalytic performance to AC. One the other hand, since the metal content is very low, the carbon nanotube growth also may be promoted surface oxygen on the AC,⁵⁶ besides the existing trace metal. Therefore, on the whole, by employing the facile mechanical milling and subsequent solid pyrolysis approach, the N-doped AC-based hybrid nanostructure decorated with nanotubes has been fabricated.

The structures of the N-doped AC-based hybrid nanoarchitecture as well as the parent AC were further characterized by XRD technique. From Fig. 5, for the two samples, the diffraction peaks towards (002) and (100) can be identified,^{41,52} indicating the well-formed graphitic structure. In circumspective comparison of the (002) peaks appear on AC and the as-prepared N-doped AC-based hybrid structure, the broader width at half maximum for the latter can be observed, suggesting smaller graphitic crystallite size. The interplane spacing of (002) crystal lattice for N-doped AC-based hybrid structure is 0.34 nm, in agreement with the interlayer distance of graphite and as well as with d spacing shown in the HRTEM image (Fig. 4). However, the 0.44 nm of larger crystal lattice for AC can be obtained.

Raman was used to further examine the structure of AC and the as-prepared N-doped AC-based hybrid structure, as well as detect the doping effect of heteroatoms. From Fig. 6, we could observe that there are two main first-order Raman modes at around 1334-1337 and 1596 cm⁻¹, corresponding to A1g mode in

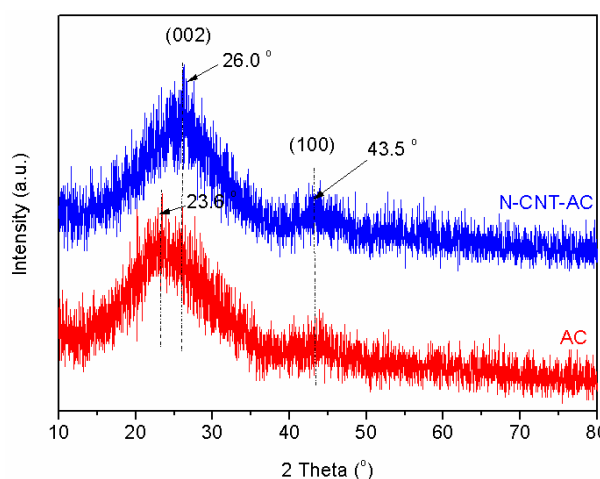


Fig. 5 XRD patterns of the as-prepared N-doped AC-based hybrid nanostructure and the parent AC.

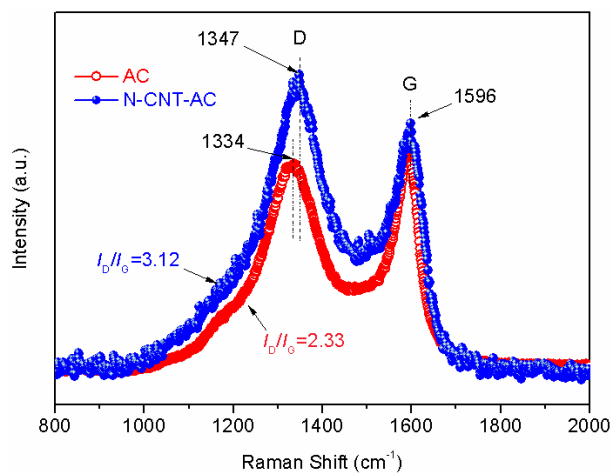


Fig. 6 Raman spectra of the as-prepared N-doped AC-based hybrid nanostructure and the parent AC.

disorder carbon or structural defect and to E 2g mode ideal graphitic carbon, respectively.⁵⁷⁻⁵⁹ The increasing intensity of the Raman spectra bands of N-doped AC-based hybrid structure in contrast to the parent AC demonstrates the intensified graphitic feature of the as-prepared hybrid composite from AC.^{57,58} Moreover, we can find that the D-band shifts from 1334 to 1347 cm^{-1} in comparison to that of parent AC while almost no change in G-band, ascribed to the doping effect of N into carbon matrix.^{30-35,57-60} The larger ID/IG (the area ratio of D peak to G peak) of N-doped AC-based hybrid structure (3.12) than that of AC (2.33) is an indicator of more structural defect and lattice edge of the as-prepared hybrid composite,⁶¹⁻⁶³ but not for more disorder amorphous carbon since the composite was prepared from AC through pyrolysis at 850 °C (less amorphous carbon but more graphitic one of the hybrid material than that of AC can be identified from the more intense G-band of the hybrid composite than that of AC). The in-plane crystallite size (L_a) of N-doped AC-based hybrid nanostructure and parent AC can be estimated by the following equation:^{61,62} L_a (nm) = $(2.4 \times 10^{-10})\lambda^4(I_D/I_G)^{-1}$ where λ is the Raman excitation wavelength (532 nm). The crystallite size towards hybrid composite (6.2 nm) is smaller than that of the parent AC (8.3 nm), in agreement with the result from XRD. The broader D bond on the hybrid composite than on the parent AC might be ascribed to small graphitic crystallite and high proportions of edge planes in the carbon nitride nanostructures. The N-doping effect, more structural defect sites, and the smaller crystallite size may allow it to exhibit much superior catalysis.

Surface chemistry of the fabricated N-doped AC-based hybrid material

Besides the structure feature, the surface chemistry of carbon materials is a significant factor affecting its catalysis.^{41,51-55} Herein, the FT-IR and XPS were employed to investigate the surface chemistry of the fabricated N-doped AC-based hybrid nanostructure, and the parent AC was also included for comparison. Fig. 7 shows the FT-IR spectra of the parent AC and the N-doped AC-based hybrid composite from AC. From Fig. 7, on the FT-IR spectra of the as-prepared N-doped AC-based hybrid nanostructure, the peaks appearing around at 760, 802, 1314, 1456 cm^{-1} correspond to the typical stretching modes of C-

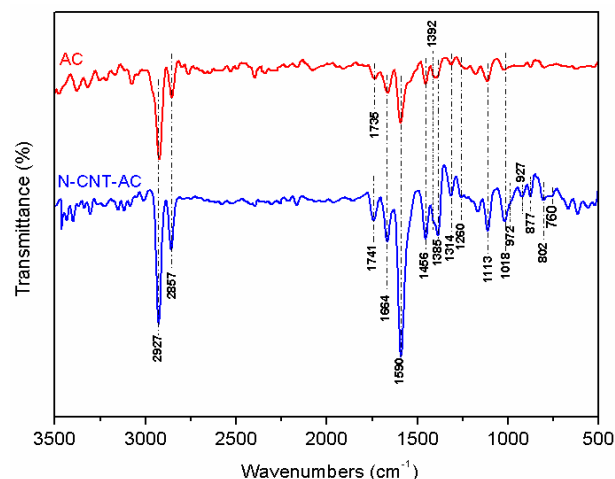


Fig. 7 FT-IR spectra of the as-prepared N-doped AC-based hybrid nanostructure and the parent AC.

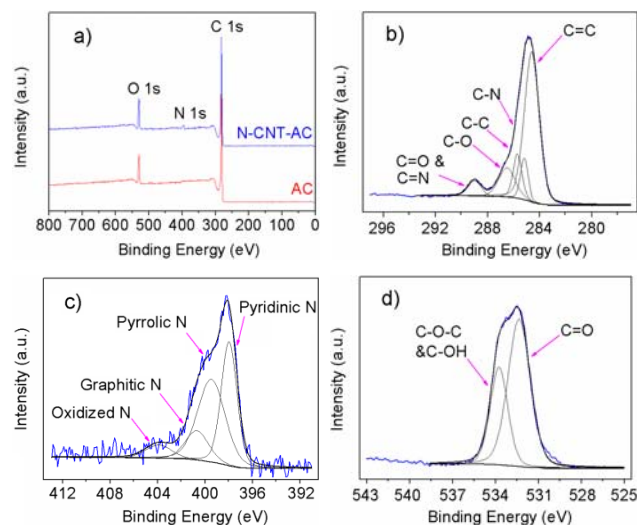


Fig. 8. XPS spectra of the as-prepared N-doped AC-based hybrid nanostructure: a) Survey spectra (the parent AC was included for comparison); b-d) C 1s, N 1s, O 1s, respectively.

N in N-containing heterocycles,^{41,52,58,64} as well as those appearing at 877, 927, and 1392 cm^{-1} are attributed to N-H deformation in-plane and out-of-plane vibration,⁶⁴ which demonstrates the formation of CN_x structure on AC. The peaks at 1020, 1113, 1260, 1385, and 1456 cm^{-1} can be indexed as C-O in C-O-C and C-OH.^{41,51,51} 1180 cm^{-1} can be indexed as the C-O stretch in phenolic group.²¹ The peaks at 1741 cm^{-1} correspond to the stretching modes of C=O in carbonyl groups.^{41,52} The carbonyl group has substantial electron density at the oxygen atom, and thus can serve as Lewis base to activate C-H bond in the DDH reaction, however phenolic hydroxyl serves as Brønsted acidic sites to enhance cracking side reaction of ethylbenzene to form benzene and toluene.^{8,41,51,52,54} The large amount of carbonyl group and the increased electron density is favourable for the desired DDH reaction. The increased basic properties via N-introducing into the hybrid may intensify the C-H bond activation, and therefore the DDH reaction can be enhanced. For both of samples, the peak around 1590 cm^{-1} is attributed to C=C stretching vibration, which shows the presence of aromatic rings. The peaks at 1735 cm^{-1} on the FT-IR of AC may be assigned to C=O in carbonyl group or in

Table 1 N content from CHN elemental analysis and relative integrated intensity of deconvoluted N 1s and O 1s XPS spectra for the as-prepared N-doped AC-based hybrid nanostructure (N-CNT-AC) and the parent AC.

Sample	N ^a (%)	N-1 ^b (%)	N-2 ^b (%)	N-3 ^b (%)	N-4 ^b (%)	O ^c (%)	C=O (%)	C-O (%)
N-CNT-AC	5.4	37.1	43.2	13.0	6.7	11.1	65.5	34.5
AC	0.1	38.1	0	49.0	12.9	9.9	11.0	89.0

^aThe total N content measured by elemental analysis. ^bPercentage of various nitrogen species occupying in the total N content; N-1, N-2, N-3, and N-4 are denoted as pyridinic N, pyrrolic N, graphitic N, and oxidized N, respectively. ^cO atom molar percentage on the material surface from XPS analysis.

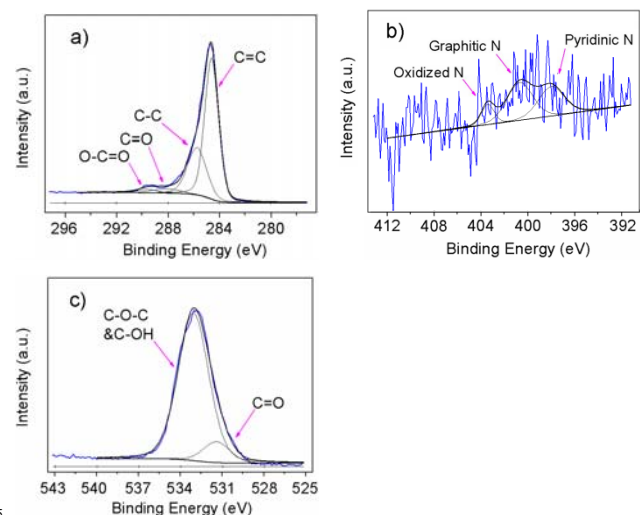


Fig. 9 The XPS spectra of the parent AC: a) C 1s, b) N 1s, c) O 1s.

carboxyl group.^{41,52} The possible COOH group may lead to the above cracking side reaction,^{41,51,52,54} which may be one reason for poor selectivity for DDH reaction.

Furthermore, the nature and coordination of the carbon, nitrogen, and oxygen in the fabricated N-doped AC-based hybrid nanoarchitecture and the parent AC were examined by XPS.^{19,41,52,61} The XPS survey spectra (Fig. 8a) of the hybrid composite shows visible signal from N element, besides strong signals from C and O, which suggests the N-introducing into the hybrid matrix. The C 1s peak region in the XPS spectrum of N-doped AC-based hybrid nanomaterial (Fig. 8b) was deconvoluted to five peaks at around 284.6, 285.2, 285.7, 286.5, and 288.8 eV assigned to C=C, C-N, C-C, C-O, and C=O/C=N, respectively.^{61,66,67} However, from the XPS spectrum of the parent AC shown in Fig. 9a, no C-N or C=N but O-C=O can be observed, further indicating N introduction into the as-synthesized hybrid material. The N into the hybrid material may promote the catalytic activation and improve selectivity of direct dehydrogenation, however the existing O-C=O on AC may lead to low selectivity for the desired reaction. The N 1s spectrum (Fig. 8c) are deconvoluted into four peaks with binding energies of 398.0, 399.4, 400.7, and 403 eV those correspond to pyridinic N, pyrrolic N, graphitic N and oxidized N, respectively,^{61,66-68} which is different from our previously reported the absence of graphitic N on the mesoporous C₃N₄ or the nanodiamond@carbon nitride hybrid nanoarchitecture. It can be proposed that the graphitic N (13.0%, Table 1) of the N-doped AC-based hybrid nanostructure may be resulted from the CN_x nanosheet or nanotube structure

that confirmed by TEM characterization. From Fig. 9b, the trace N exists in the AC (0.1 wt% from Table 1 measured by elemental analysis), however, the 5.4 wt% N content in the N-doped AC-based hybrid structure. The higher N content in the materials is favorable for the DDH reaction.^{41,52} The O 1s XPS spectrum can be deconvoluted into two peaks with the binding energies of 532.4 and 533.8 eV, assigned to C=O and C-O-C/C-OH containing groups (Fig. 8d, Fig. 9c, and Table 1).^{69,70} From Table 1, the as-prepared N-doped AC-based hybrid composite only has a little higher O content on its surface than the parent AC (the increased oxygen content in N-CNT-AC than that in AC may be resulted from the inhibition effect of adding melamine on the oxygen atom leaving from AC surface in the high temperature calcination procedure). However, the O 1s spectrum towards N-doped AC-based hybrid composite (Fig. 8d) is significantly different from that of the parent AC (Fig. 9c), the C=O is the main form of oxygen atom in the hybrid composite, but C-O-C/C-OH in the AC (Table 1). The dominant C=O group in the developed hybrid nanostructure may allow it to show much superior catalytic performance including activity and selectivity for C=O group-activated reactions like oxidation, dehydrogenation, and hydrogen-transferring reactions, however, the rich C-OH groups on the AC surface would lead to low selectivity for DDH reaction by the formation of benzene and toluene obtained from the possible acid-catalyzed cracking.

60 Catalytic properties of N-doped AC-based hybrid material

Direct dehydrogenation of ethylbenzene is an extremely important reaction for industrial production of the large amount-required styrene. From the viewpoint of sustainable development, the carbocatalysts are fascinating candidates. However, current efforts are mainly focused on carbon catalyzed oxidative dehydrogenation,^{8,9,71} and rare report on carbocatalyzed oxygen- and steam-free direct dehydrogenation can be found.^{41,51,52} Therefore, to develop oxygen- and steam-free dehydrogenation process catalyzed by nanocarbon is highly desirable but remains a rigorous challenge.

AC is a low-cost, abundant, sustainable, and commercially large-scale available common carbon material. Once the highly active and selective AC-based catalyst can be developed by a facile approach, it would be considered to be a practical and highly-efficient candidate for industrial application. Herein, we evaluated the catalytic properties of the fabricated N-doped AC-based hybrid composite for the DDH of ethylbenzene to produce styrene under oxidant- and steam-free conditions, and the parent AC, mpg-C₃N₄ (MCN-1) as well as the industrially-used K-Fe catalyst were included for comparison. The styrene rate and selectivity towards styrene as a function of time on stream are presented in Fig. 10. The results demonstrate that the developed N-doped AC-based hybrid nanostructure exhibits superior steady-state styrene rate (2.46 mmol g⁻¹ h⁻¹) and selectivity (94.7%) to the other samples. The common, low-cost and renewable but highly active and selective AC-based catalyst exhibits 3.67 times the steady-state styrene rate of the industrially-used K-Fe catalyst for DDH reaction with similar selectivity, which makes it an industrially potential candidate for styrene production via DDH reaction of ethylbenzene. Although the developed AC-based hybrid has a 397.0 cm² g⁻¹ of low surface area (surface area for AC is 777.1 m² g⁻¹), the as-prepared N-doped AC-based hybrid

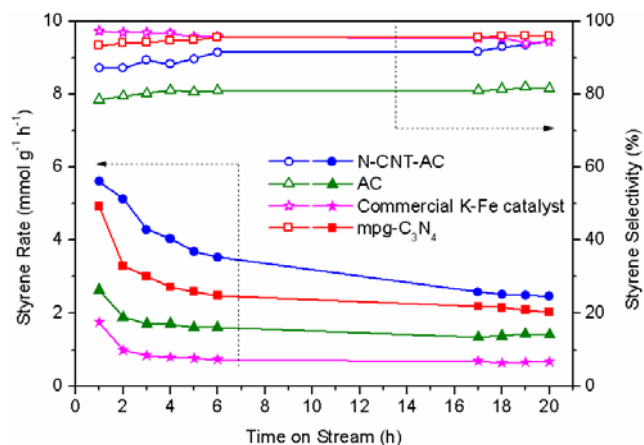


Fig. 10 Catalytic performance of N-doped AC-based hybrid nanostructure, the parent AC, mpg-C₃N₄ (MCN-1), and the commercially used K-Fe catalyst as a function of time on stream for metal-free direct dehydrogenation of ethylbenzene to styrene under oxidant- and steam-free conditions.

nanostructure exhibits much superior catalytic activity to the parent AC, as well as our previously reported mesoporous C₃N₄, ascribed to the unique microstructure and the special surface chemistry.

More interestingly, the significantly improved selectivity of the AC by the fabrication of AC-based N-doped AC-based hybrid nanostructure can be clearly seen, which may be resulted from the improved basicity, and electron density and electron conductivity by nitrogen introduction into the carbon matrix. The main byproducts for the catalytic direct dehydrogenation of ethylbenzene are benzene and toluene resulted from the cracking of ethylbenzene, which consists with the results reported in literatures.^{41,51,52} In comparison of the N-doped AC-based hybrid nanostructure with parent AC, the former exhibits significantly superior catalytic performance especially the selectivity. The C=O can be the catalytic active species, which serves as Lewis bases to activate saturated hydrocarbon for this dehydrogenation reaction has been confirmed,^{8,41,51,52} the surface phenolic hydroxyl group and/or possible COOH may enhance the cracking of ethylbenzene due to its acidity, since acid sites are active for cracking reaction of hydrocarbon.⁵⁴ The introduction of nitrogen atom into hybrid composite can increase the electron density of carbon materials, and therefore strengthens the basicity but weakens the acidity of the catalyst, which may result in an improvement in catalytic activity for styrene production and simultaneously compressing the benzene and toluene formation. As a result, the superior catalytic activity and selectivity over N-doped AC-based hybrid nanostructure to the parent AC can be demonstrated.

Correlated to characterization results from TEM, XRD, UV Raman, FT-IT, and XPS presented as above, we successfully fabricated the N-doped AC-based hybrid nanostructure, and its excellent catalytic performance in DDH reaction can be ascribed to the promotion effect of the unique nanostructures (microstructure effect), surface rich C=O group and defect/edge feature, the increased basic properties through N-introducing into the hybrid nanostructure, small size of graphitic crystallites, as well as the inherent high surface and large porosity of AC-based materials.

Activation energy measurement via in situ FT-IR

Furthermore, in situ FT-IR experiments on the ethylbenzene-adsorbed samples as a function of temperature from 150 to 400 °C were performed to measure the activation energy of the as-fabricated N-doped AC-based hybrid nanostructure and the parent AC for DDH reaction of ethylbenzene to produce styrene under oxidant- and steam-free conditions. The FT-IR spectra are presented in Fig. 11. In the in situ FT-IR spectra, the peak at around 910 cm⁻¹ can be assigned to the C-H out-of-plane mode of the vinyl group =CH₂,^{72,73} which can be considered as an indication for the styrene formation. From Fig. 11, the temperature for the initial formation of styrene on the developed N-doped AC-based hybrid nanostructure and the parent AC are 210 and 330 °C, respectively, demonstrating the lower activation energy for the direct dehydrogenation of ethylbenzene to styrene over the fabricated N-doped AC-based hybrid nanostructure, which is in consistent with the reaction results shown in Fig. 10. Owing to the unique nanostructure of the hybrid composites formed by carbon nitride nanosheets coating AC decorated with carbon nitride nanotubes, the introduction of nitrogen, C=O group- and defect-rich surface nature, small graphitic crystallite size, as well as the inherent high surface and large porosity of the parent AC, the fabricated AC-based N-doped AC-based hybrid nanoarchitecture has demonstrated the outstanding catalytic performance. Take low-cost, abundant resource, large commercial-availability, and the superior catalytic performance into account, the developed AC-based N-doped AC-based hybrid

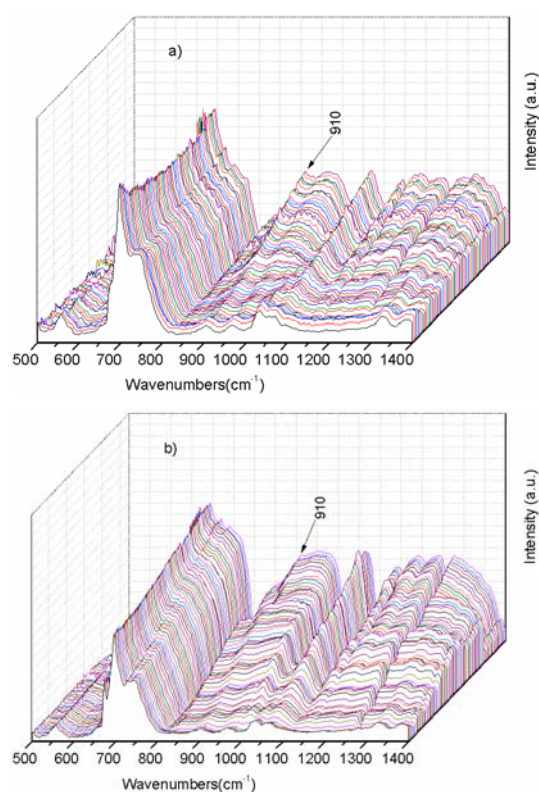


Fig. 11 In situ FT-IR spectra of the as-prepared N-doped AC-based hybrid nanostructure (a) and the parent AC (b) adsorbed ethylbenzene as a function of temperature. The initial temperatures for styrene formation over the developed N-doped AC-based hybrid nanostructure and AC are 210 and 330 °C, respectively.

nanostructure could be a practical catalyst for industrial applications in styrene production.

Conclusions

In this work, on the basis of the abundant, low-cost, sustainable parent AC, we have successfully fabricated N-doped AC-based hybrid nanostructure decorated with nanotubes by a facile and scalable mechanical milling and subsequent controllable pyrolysis approach. The fabricated carbon hybrid material exhibits much superior catalytic performance to the parent and even to our previously reported mesoporous carbon nitride including activity and selectivity, ascribed to the promotion effect of the formed unique nanostructures, surface rich C=O group and defect/edge feature, the increased basic properties through N-introducing into the hybrid nanostructure, small size of graphitic crystallite, as well as the inherent high surface and large porosity of AC-based materials. Owing to the abundance, low-cost, sustainability of the parent AC, and the excellent catalytic performance, as well as the low-cost, facile and easy realization of large-scale production approach, the fabricated N-doped AC-based hybrid nanostructure could be a practical metal-free catalyst for catalyzing the DDH reaction of ethylbenzene to styrene under oxidant- and steam-free conditions. The unique nanostructure and surface chemistry of the AC-based nanostructure allow it to be a fascinating candidate for diverse applications in catalysis, as solar cell, CO₂ capture, hydrogenation storage, supercapacitor, oxygen reduction, etc.

Acknowledgments

This work is financially supported by the National Natural Science Foundation of China (grant no. 20803006, 21276041, and U1261104), also sponsored by the Chinese Ministry of Education via the Program for New Century Excellent Talents in University (Grant no. NCET-12-0079).

Notes and references

State Key Laboratory of Fine Chemicals, Department of Catalysis Chemistry and Engineering, School of Chemical Engineering, Dalian University of Technology, Dalian 116024, P.R. China. E-mail: zkzhao@dlut.edu.cn; Fax: +86-411-84986354

- M. S. Chen and M. C. White, *Science*, 2010, **327**, 566-571.
- Y. H. Li, S. Das, S. L. Zhou, K. Junge and M. Beller, *J. Am. Chem. Soc.*, 2012, **134**, 9727-9732.
- Q. S. Gao, C. Giordano and M. Antonietti, *Angew. Chem. Int. Ed.*, 2012, **51**, 11740-11744.
- D. R. Dreyer and C. W. Bielawski, *Chem. Sci.*, 2011, **2**, 1233-1240.
- C. Su and K. P. Loh, *Acc. Chem. Res.*, 2013, **46**, 2275-2285.
- X. Sun, R. Wang and D. S. Su, *Chin. J. Catal.*, 2013, **34**, 508-523.
- Schaetz A, Zeltner M and Stark WJ, *ACS Catal.* 2012;**2**:1267-1284.
- J. Zhang, X. Liu, R. Blume, A. H. Zhang, R. Schlögl and D. S. Su, *Science*, 2008, **322**, 73-77.
- W. Qi, W. Liu, B. Zhang, X. Gu, X. Guo and D. S. Su, *Angew. Chem. Int. Ed.*, 2013, **52**, 14224-14228.
- Y. Gao, G. Hu, J. Zhong, Z. Shi, Y. Zhu, D. S. Su, J. Wang, X. Bao and D. Ma, *Angew. Chem. Int. Ed.*, 2013, **52**, 2109-2113.
- S. P. Pitre, C. D. McTiernan, H. Ismaili and J. C. Scaiano, *J. Am. Chem. Soc.*, 2013, **135**, 13286-13289.
- Y. Wang, X. Wang and M. Antonietti, *Angew. Chem. Int. Ed.*, 2012, **51**, 68-89.
- J. Bedia, R. Ruiz-Rosas, J. Rodríguez-Mirasol and T. Cordero, *AIChE J.*, 2010, **56**, 1557-1568.
- P. Ji, H. Tan, X. Xu and W. Feng, *AIChE J.*, 2010, **56**, 3005-3011.
- K. Schwinghammer, B. Tuffy, M. B. Mesch, E. Wirnhier, C. Martineau, F. Taulelle, W. Schnick, J. Senker and B. V. Lotsch, *Angew Chem Int Ed.* 2013, **52**, 2435-2439.
- M. Younessi-Sinaki and F. Hamdullahpur, *AIChE J.*, 2014, **60**, 2228-2234.
- M. Shalom, S. Inal, C. Fettkenhauer, D. Neher and M. Antonietti, *J. Am. Chem. Soc.*, 2013, **135**, 7118-7121.
- Y. S. Jun, E. Z. Lee, X. Wang, W. H. Hong, G. D. Stucky and A. Thomas, *Adv. Funct. Mater.*, 2013, **23**, 3661-3667.
- Y. Zheng, Y. Jiao, Y. L. Ge, M. Jaroniec and S. Z. Qiao, *Angew. Chem. Int. Ed.*, 2013, **52**, 3110-3116.
- Y. Zhao, L. Yang, S. Chen, X. Wang, Y. Ma, Q. Wu, Y. Jiang, W. Qian and Z. Hu, *J. Am. Chem. Soc.*, 2013, **135**, 1201-1204.
- K. Ai, Y. Liu, C. Ruan, L. Lu and G. Lu, *Adv. Mater.*, 2013, **25**, 998-1003.
- H. Wang, K. Sun, F. Tao, D. J. Stacchiola and Y. H. Hu, *Angew. Chem. Int. Ed.*, 2013, **52**, 9210-9214.
- I. V. Lightcap and P. V. Kamat, *Acc. Chem. Res.*, 2013, **46**, 2235-2243.
- V. J. Watson, C. N. Delgado and B. E. Logan, *Environ. Sci. Technol.* 2013, **47**, 6704-6710.
- V. M. Mohan, K. Murakami, A. Kono and M. Shimomura, *J. Mater. Chem. A.*, 2013, **1**, 7399-7407.
- W. Xing, C. Liu, Z. Zhou, L. Zhang, J. Zhou, S. Zhuo, Z. Yan, H. Gao, G. Wang and S. Z. Qiao, *Energy Environ. Sci.*, 2012, **5**, 7323-7327.
- M. Sevilla and R. Mokaya, *Energy Environ. Sci.* 2014, **7**, 1250-1280.
- J. P. S. Sousa, M. F. R. Pereira and J. L. Figueiredo, *Catal. Today.*, 2011, **176**, 383-387.
- B. Zhang, Z. Wen, S. Ci, S. Mao, J. Chen and Z. He, *ACS Appl. Mater. Interfaces.*, 2014, **6**, 7464-7470.
- V. Calvino-Casilda, A. J. López-Peinado, C. J. Durán-Valle and R. M. Martín-Aranda, *Catal. Rev.*, 2010, **52**, 325-380.
- Z. K. Zhao, H. L. Yang, Y. Li and X. W. Guo, *Green Chem.*, 2014, **16**, 1274-1281.
- Z. K. Zhao, H. L. Yang and Y. Li, *RSC Adv.*, 2014, **4**, 22669-22677.
- T. Bao, Z. K. Zhao, Y. Dai, X. L. Lin, R. H. Jin, G. R. Wang and T. Muhammad, *Appl. Catal. B: Environ.*, 2012, **119-120**, 62-73.
- Z. K. Zhao, T. Bao, Y. Zeng, G. R. Wang and T. Muhammad, *Catal. Commun.*, 2013, **32**, 47-51.
- L. Degirmenci, N. Oktar and G. Dogu, *AIChE J.*, 2011, **57**, 3171-3181.
- I. Gniot, P. Kirszenstejn and M. Kozłowski, *Appl. Catal. A: Gen.*, 2009, **362**, 67-74.
- A. Malaika, P. Rechnia, B. Krzyżyńska, A. Tolińska, A. Kawalko and M. Kozłowski, *Appl. Catal. A: Gen.*, 2013, **452**, 39-47.
- I. Velo-Gala, J. J. López-Peñalver, M. Sánchez-Polo and J. Rivera-Utrilla, *Appl. Catal. B: Environ.*, 2013, **142-143**, 694-704.
- N. Brun, S.A. Wohlgenuth, P. Osiceanu and M. M. Titirici, *Green Chem.*, 2013, **15**, 2514-2524.
- J. Zhang, D. Su, A. Zhang, D Wang, R. Schlögl and C. Hébert, *Angew. Chem. Int. Ed.*, 2007, **46**, 7319-7323.
- Z. K. Zhao and Y. T. Dai, *J. Mater. Chem. A.*, 2014, **2**, 13442-13451.
- E. H. Lee, *Catal. Rev.*, 1973, **8**, 285-305.
- F. Cavani and F. Trifiro, *Appl. Catal. A: Gen.*, 1995, **133**, 219-239.
- A. P. Addiego, C. A. Estrada, D. W. Goodman and M. P. Rosynek, *J. Catal.*, 1994, **146**, 407-414.
- Y. Ohishi, T. Kawabata, T. Shishido, K. Takaki, Q. Zhang, Y. Wang, K. Nomura and K. Takehira, *Appl. Catal. A: Gen.*, 2005, **288**, 220-231.
- R. J. Balasamy, A. Khurshid, A. S. S. Al-Ali, L. A. Atanda, K. Sagata, M. Asamoto, H. Yahiro, K. Nomura, T. Sano, K. Takehira and S. S. Al-Khattaf, *Appl. Catal. A: Gen.*, 2010, **390**, 225-234.
- O. Shekha, W. Ranke and R. Schlögl, *J. Catal.*, 2004, **225**, 56-60.
- J. J. Serra, A. Corma, D. Farrusseng, L. Baumes, C. Mirodatos, C. Flego and C. Perego, *Catal. Today*, 2003, **81**, 425-436.
- D. S. Su, N. Maksimova, J. J. Delgado, N. Keller, G. Mestl, M. J. Ledoux and R. Schlögl, *Catal. Today*, 2005, **102-103**, 110-114.
- D. S. Su, N. I. Maksimova, G. Mestl, V. L. Kuznetsov, V. Keller, R. Schlögl and N. Keller, *Carbon*, 2007, **45**, 2145-2151.

51. J. Zhang, D. S. Su, R. Blume, R. Schlögl, R. Wang, X. Yang and A. Gajović, *Angew. Chem. Int. Ed.*, 2010, **49**, 8640-8644.
52. Z. K. Zhao, Y. T. Dai, J. H. Lin and G. R. Wang, *Chem. Mater.*, 2014, **26**, 3151-3161.
53. X. Jin, V. V. Balasubramanian, S. T. Selvan, D. P. Sawant, M. A. Chari, G. Q. Lu and A. Vinu, *Angew. Chem. Int. Ed.*, 2009, **48**, 7884-7887.
54. Y. V. Kissin, *Catal. Rev.*, 2001, **43**, 85-146.
55. J. Lu, L. Yang, B. Xu, Q. Wu, D. Zhang, S. Yuan, Y. Zhai, X. Wang, Y. Fan and Z. Hu, *ACS Catal.*, 2014, **4**, 613-621.
56. B. Liu, D. M. Tang, C. Sun, C. Liu, W. Ren, F. Li, W. J. Yu, L. C. Yin, L. Zhang, C. Jiang and H. M. Cheng, *J. Am. Chem. Soc.*, 2011, **133**, 197-199.
57. Y. Xia and R. Mokaya, *Chem. Mater.*, 2005, **17**, 1553-1560.
58. V. N. Khabashesku, J. L. Zimmerman and J. L. Margrave, *Chem. Mater.*, 2000, **12**, 3264-3270.
59. R. Silva, J. Al-Sharab and T. Asefa, *Angew. Chem. Int. Ed.*, 2012, **51**, 7171-7175.
60. Y. Xia and R. Mokaya, *Adv. Mater.*, 2004, **16**, 1553-1558.
61. Z. Lin, G. Waller, Y. Liu, M. Liu and C. P. Wong, *Adv. Energy Mater.*, 2012, **2**, 884-888.
62. P. Wu, Y. Qian, P. Du, H. Zhang and C. Cai, *J. Mater. Chem.*, 2012, **22**, 6402-6412.
63. H. Muramatsu, K. Fujisawa, Y. I. Ko, K. S. Yang, T. Hayashi, M. Endo, C. M. Yang, Y. C. Jung and Y. A. Kim, *Chin. J. Catal.*, 2014, **35**, 864-868.
64. G. H. Jun, S. H. Jin, B. Lee, B. H. Kim, W. S. Chae, S. H. Hong and S. Jeon, *Energy Environ. Sci.*, 2013, **6**, 3000-3006.
65. L. Liu, Q. F. Deng, T. Y. Ma, X. Z. Lin, X. X. Hou, Y. P. Liu and Z. Y. Yuan, *J. Mater. Chem.*, 2011, **21**, 16001-16009.
66. N. Jung, S. Kwon, D. Lee, D. M. Yoon, Y. M. Park, A. Benayad, J. Y. Choi and J. S. Park, *Adv. Mater.*, 2013, **25**, 6854-6858.
67. L. Shang, T. Bian, B. Zhang, D. Zhang, L. Z. Wu, C. H. Tung, Y. Yin and T. Zhang, *Angew. Chem. Int. Ed.*, 2014, **53**, 250-254.
68. W. Ding, Z. Wei, S. Chen, X. Qi, T. Yang, J. Hu, D. Wang, L. J. Wan, S. F. Alvi and L. Li, *Angew. Chem. Int. Ed.*, 2013, **52**, 11755-11759.
69. Y. Hou, Z. Wen, S. Cui, X. Guo and J. Chen, *Adv. Mater.*, 2013, **25**, 6291-6297.
70. T. N. Huan, T. V. Khai, Y. Kang, K. B. Shim and H. Chung, *J. Mater. Chem.*, 2012, **22**, 14756-14762.
71. W. P. Addiego, C. A. Estrada, D. W. Goodman, M. P. Rosynek and R. G. Windham, *J. Catal.*, 1994, **147**, 407-414.
72. L. Liu, Q. F. Deng, B. Agula, X. Zhao, T. Z. Ren and Z. Y. Yuan, *Chem. Commun.*, 2011, **47**, 8334-8336.
73. R. Rao, M. Yang, Q. Ling, C. Li, Q. Zhang, H. Yang and A. Zhang, *Catal. Sci. Technol.*, 2014, **4**, 665-671.